Light Resonances in $K_S^0 K^\pm \pi^\mp$ and $\eta\pi^+\pi^-$ final states in $\gamma\gamma$ collisions at LEP

The L3 Collaboration

Abstract

The $e^+e^- \to e^+e^- K_S^0 K^\pm \pi^\mp$ and $e^+e^- \to e^+e^-\eta\pi^+\pi^-$ final states are studied with the L3 detector at LEP using data collected at centre–of–mass energies from 183 GeV up to 202 GeV. The mass spectrum of the $K_S^0 K^\pm \pi^\mp$ final state shows an enhancement around 1470 MeV, which is identified with the pseudoscalar meson $\eta(1440)$. This state is observed in $\gamma\gamma$ collisions for the first time and its two–photon width is measured to be $\Gamma_{\gamma\gamma}\big(\eta(1440)\big) \times \mathrm{BR}\big(\eta(1440) \to K\bar{K}\pi\big) = 212 \pm 50$ (stat.) $\pm$ 23 (sys.) eV. Clear evidence is also obtained for the formation of the axial vector mesons $f_1(1420)$ and $f_1(1285)$. In the $\eta\pi^+\pi^-$ channel the $f_1(1285)$ is observed, and upper limits for the formation of $\eta(1440)$ and $\eta(1295)$ are obtained.

1   Introduction

Resonance formation in two–photon interactions offers a clean environment to study the spectrum of mesonic states. In this paper we study the reactions $\gamma\gamma \to K^0_S K^\pm \pi^\mp$ and $\gamma\gamma \to \eta\pi^+\pi^-$.

The mass region between 1200 MeV and 1500 MeV is expected to contain several states [1]. For the pseudoscalar sector ($J^{PC} = 0^{-+}$), the $\eta(1440)$ meson, formerly known as E or ι, is expected to be seen. The $\eta(1440)$ was observed in hadron collisions and in radiative J decay, but not in two–photon collisions, and only upper limits of its two–photon width, $\Gamma_{\gamma\gamma}$, of the order of 1 keV exist [2,3]. Therefore the $\eta(1440)$ may be interpreted as a prominent glueball candidate due to its strong production in a gluon rich environment. There are, possibly, two pseudoscalars [4] in the 1440 MeV mass region: one at lower mass, η_L, which decays into $a_0\pi$ or directly into $\eta\pi\pi$, and another at higher mass, η_H, decaying to K^*K. The average masses and widths for these states [1] are listed in Table 1. Taking into account also the $\eta(1295)$, there are therefore three candidates for the first radial excitations of the pseudoscalar SU(3) nonet. If one of these states is a gluonium, its two–photon width is expected to be small with respect to a q$\bar{q}$ state. However, the gluonium interpretation is disfavoured by lattice gauge theories [5] which predict the lowest lying 0^{-+} gluonium state to be above 2 GeV. More exotic interpretations such as a bound state of gluinos [6] are also proposed.

Axial vector mesons ($J^{PC} = 1^{++}$) are also present in these final states in the 1440 MeV mass region. The $f_1(1420)$ was observed in two–photon collisions, in the $K\bar{K}\pi$ decay channel, by the CELLO [3], TPC–2γ [7], JADE [8] and Mark II [9] Collaborations, the $f_1(1285)$ was seen [7,9] in the $\eta\pi^+\pi^-$ decay channel.

The data used here were collected by the L3 detector [10] at LEP from 1997 to 1999 at centre–of–mass energies between 183 GeV and 202 GeV, corresponding to a total integrated luminosity of 449 pb^{-1}. These events were collected by the track triggers [11]. The analysis makes use of the dependence of the signal yield on the total transverse momentum $P_T^2 = (\sum \vec{p_T})^2$, where the sum runs over all the observed particles. To a good approximation $P_T^2 = Q^2$, where Q^2 is the maximum virtuality of the two photons. According to the Landau–Yang theorem [12], for real photons ($Q^2 \simeq 0$), the production of a spin-0 state is allowed while that of a spin-1 state is suppressed. In contrast, for virtual photons ($Q^2 > 0$), the production of a spin-1 state is allowed while that of a spin-0 state diminishes. Such behaviour is described by the effective form factors for the pseudoscalar and axial vector mesons. The form factors as a function of Q^2 calculated [13] for the $\eta(1440)$ and for the $f_1(1420)$ are shown in Figure 1. The difference at $Q^2 \simeq 0$ is clearly seen.

2   Monte Carlo

Two Monte Carlo generators are used to describe two–photon resonance formation: EGPC [14] and GaGaRes [15]. The EGPC Monte Carlo describes the two–photon process as the product of the luminosity function for transverse photons [16] and the resonance production cross section. The latter is generated according to a Breit–Wigner function with $\Gamma_{\gamma\gamma} = 1$ keV. The ratio of the measured cross section to that obtained with the Monte Carlo integration then gives $\Gamma_{\gamma\gamma}$. The decay of the resonance is generated according to Lorentz invariant phase space.

Events are generated for all the resonances of interest. For the $K^0_S K^\pm \pi^\mp$ channel this is done for masses of 1410 MeV, 1440 MeV and 1480 MeV and a full width of 50 MeV. For the $\eta\pi^+\pi^-$ channel, resonances are generated for the mass 1285 MeV with a full width of 20 MeV as well as for masses of 1405 MeV and 1440 MeV with 50 MeV full width.

To take into account the Q^2 dependence of pseudoscalar and axial vector mesons, EGPC events are re–weighted according to the prediction of GaGaRes. This uses the exact matrix element for resonance production, $e^+e^- \to e^+e^-R$, obtained from the hard scattering approach [13].

The generated events are passed through the L3 detector simulation based on the GEANT [17] and GEISHA [18] programs. Time dependent detector inefficiencies, as monitored during the data taking period, are also simulated.

3 The $e^+e^- \to e^+e^- K_S^0 K^\pm \pi^\mp$ channel

3.1 Event selection

Events are selected by requiring four charged particles in the central tracker, two tracks ($K^\pm \pi^\mp$), coming from the interaction point, and a K_S^0 decaying into $\pi^+\pi^-$ at a secondary vertex. For charged particle identification, consistency of the corresponding dE/dx measurement, with a confidence level CL>1%[1]), is required.

Events with photons are rejected where a photon is defined as an energy deposition in the electromagnetic calorimeter of more than 100 MeV in the polar angular range $0.21 < \theta < 2.93$ rad. No track should lie within 0.2 rad from the photon direction.

The $K_S^0 \to \pi^+\pi^-$ is identified by:

- a secondary vertex at least 3 mm away, in the transverse plane, from the interaction point;

- the angle α, in the transverse plane, between the flight direction of the K_S^0 candidate and the direction of the total transverse momentum vector of the two outgoing tracks being smaller than 0.2 rad;

- the momentum of the K_S^0 candidate and the distance between the primary and the secondary vertex being consistent with the K_S^0 lifetime with CL>99%;

- the effective mass of the two pions being within the mass region 0.46–0.53 GeV.

$K_S^0 K_S^0$ background, arising from K/π misidentification, is excluded by rejecting events with a second K_S^0 in the mass range 0.48–0.51 GeV. Figure 2a presents the $\pi^+\pi^-$ invariant mass spectrum for particles from the secondary vertex in events selected with $P_T^2 < 0.2$ GeV^2. A Gaussian fit of the peak gives $M = 496.7 \pm 0.6$ MeV and $\sigma = 9.0 \pm 0.7$ MeV, consistent with the K_S^0 mass and width.

The $K^\pm \pi^\mp$ identification requires that:

- the two tracks lie within three standard deviations from the interaction point both in the transverse plane and along the beam axis;

- their dE/dx measurement must be consistent with a $K^\pm \pi^\mp$ hypothesis, with the combined confidence level CL($K^\pm \pi^\mp$) > 1%. A pion is identified if $\chi^2_{dE/dx}(\pi^\pm) < \chi^2_{dE/dx}(K^\pm) - 4$ and a kaon if $\chi^2_{dE/dx}(K^\pm) < \chi^2_{dE/dx}(\pi^\pm) - 4$. If the particles are not identified, both hypotheses are taken, each with a weight of 0.5.

To further improve the $K_S^0 K^\pm \pi^\mp$ selection, additional requirements are used as a function of P_T^2. For low P_T^2 the dE/dx identification has high discriminating power as shown in Figure 2b. For higher P_T^2 the dE/dx performance degrades, but the $\pi^+\pi^-\pi^+\pi^-$ background is smaller. The data are hence divided into two samples.

---

[1])A $\chi^2_{dE/dx}$ is evaluated for each particle identity, $\chi^2_{dE/dx} = (dE/dx_{measured} - dE/dx_{expected})^2 / \sigma^2_{dE/dx}$

- For $P_T^2 < 0.2$ GeV^2, the event is accepted if, at the primary vertex, the two–pion hypothesis has a low confidence level, CL$(\pi^{\pm}\pi^{\mp}) < 10^{-3}$, from the dE/dx measurement.

- For $P_T^2 > 0.2$ GeV^2, either the previous requirement is satisfied or two long tracks are reconstructed at the primary vertex and the two tracks at the secondary vertex have a probability less than 30% to come from the primary vertex.

3.2 Q^2 dependence

The selection results in the $K_S^0 K^{\pm}\pi^{\mp}$ effective mass spectra shown in Figure 3. A clear peak is seen in the 1440 MeV mass region. The data are subdivided into four P_T^2 intervals of similar statistics in the peak region, in order to study the $\eta(1440)$ and f$_1(1420)$ contributions.

A fit to a Gaussian plus second order polynomial background is performed for each P_T^2 interval. The results are listed in Table 2. For the peak in the lowest P_T^2 interval, Figure 3a, the mass and width, $M = 1481 \pm 12$ MeV and $\sigma = 48 \pm 9$ MeV, are compatible[2] with those of the η_H. In the highest P_T^2 interval, 1 GeV$^2 < P_T^2 < 7$ GeV^2, an f$_1(1285)$ signal is present, so this spectrum is fitted to two Gaussians plus a polynomial.

The acceptance of the detector, the selection and trigger efficiencies, as estimated for each P_T^2 interval, are presented in Table 2. The detector acceptance and the selection efficiency, as well as the efficiency of the central track trigger, which varies from 0.97 at low P_T^2 to 0.74 at the highest P_T^2, are determined by Monte Carlo. Inefficiencies due to the higher level triggers, evaluated directly from the data, range from 2% to 8%.

The cross section $\Delta\sigma$ for each P_T^2 interval, evaluated from the fitted number of events in the Gaussian peak, is listed in Table 2. The differential cross section $d\sigma/dP_T^2$ is shown in Figure 4. It is fitted, using the predictions for the Q^2 dependence of $\eta(1440)$ and f$_1(1420)$ production given by the GaGaRes Monte Carlo, to the following three hypotheses.

- Pure pseudoscalar $\eta(1440)$. This is excluded with a CL $\sim 10^{-3}$, due to the high number of events observed at high Q^2.

- Pure axial vector meson f$_1(1420)$. This is excluded with a CL $\sim 10^{-5}$, due to the strong peak at $Q^2 \simeq 0$.

- Simultaneous presence of the $\eta(1440)$ and f$_1(1420)$ resonances. This hypothesis leads to a CL $\simeq 9\%$, with 74 ± 10 events for the spin–0 particle and 42 ± 10 events for the spin–1.

3.3 Two–photon width

The two–photon width of the $\eta(1440)$ is determined using only the events with $P_T^2 < 0.02$ GeV^2, shown in Figure 3a. This cut selects events produced by quasi–real photons, dominated by the spin–0 state. The cross section measurement yields:

$$\Gamma_{\gamma\gamma}\big(\eta(1440)\big) \times \text{BR}\big(\eta(1440) \to K_S^0(\to \pi^+\pi^-)K^{\pm}\pi^{\mp}\big) = 49 \pm 12 \text{ (stat.) eV.}$$

The most important systematic uncertainties result from varying the dE/dx cut (5%), the P_T^2 cut (4.7%), and from the background subtraction and the shape of the resonance (8%). Using the result of the fit to the P_T^2 dependence, the contribution of the f$_1(1420)$ is estimated to be 1.5%. This contribution is not corrected for, but included in the systematic uncertainty.

---

[2]A Gaussian fit to a Breit–Wigner of $\Gamma = 80$ MeV, convoluted with the resolution function $\sigma = 20$ MeV, gives $\sigma = 47$ MeV.

Taking into account the branching ratio values [1], $BR(K_S^0 \to \pi^+\pi^-)$ and $BR(K^0 \to K_S^0)$, and the isospin factor $K\bar{K}\pi \,/\, K^0 K^\pm \pi^\mp$ the two–photon width for the $K\bar{K}\pi$ decay channel is:

$$\Gamma_{\gamma\gamma}\big(\eta(1440)\big) \times BR\big(\eta(1440) \to K\bar{K}\pi\big) = 212 \pm 50 \ \text{(stat.)} \pm 23 \ \text{(sys.)} \ \text{eV}.$$

This value is consistent with the upper limit of 1.2 keV reported by the CELLO Collaboration [3].

3.4 Intermediate states

To improve the statistics for the study of the intermediate decay states K^*K and $a_0\pi$ the transverse momentum cut is released to $P_T^2 < 0.2 \ \text{GeV}^2$. This doubles the statistics in the peak to 65 ± 11 events, as compared to the sample with $P_T^2 < 0.02 \ \text{GeV}^2$, while the contribution of $f_1(1420)$ is still only $\sim 10\%$. To search for signals due to $K^*(892)$ and $a_0(980)$, the $K\pi$ and $K_S^0 K^\pm$ mass spectra in the $\eta(1440)$ region, $1370 \ \text{MeV} < M(K_S^0 K^\pm \pi^\mp) < 1560 \ \text{MeV}$, are investigated. The results are shown in Figure 5. A clear $K^*(892)$ signal is seen in the $K_S^0 \pi^\pm$ and $K^\pm \pi^\mp$ spectra. Gaussian fits over linear backgrounds give a mass and width consistent with the $K^*(892)$. Since the $a_0(980)$ region of the $K_S^0 K^\pm$ mass lies entirely within the K^* mass bands, no exclusive selection of this decay channel is possible. The $K_S^0 K^\pm$ spectrum (Figure 5d) shows no clear evidence for the presence of the $a_0(980)$. With the present limited statistics no firm conclusion can be drawn concerning the possible presence of the $\eta_L \to a_0\pi$ state in the data.

4 The $e^+e^- \to e^+e^- \eta\pi^+\pi^-$ channel

4.1 Event selection

The η is detected via its decay $\eta \to \gamma\gamma$. The events are selected by requiring two pions of opposite charge and two photons, identified with the criteria defined in section 3.1. In addition the most energetic photon must have energy greater than 300 MeV and the effective mass of the two photons must be inside the η mass range, $0.47 - 0.62$ GeV. Also a kinematical fit, constrained to the η mass, is applied.

After these cuts, 6444 events are selected with $\eta\pi^+\pi^-$ masses below 1750 MeV. The $\eta\pi^+\pi^-$ mass spectrum, shown in Figure 6a, is dominated by the $\eta'(958)$ resonance. A Gaussian fit gives $M = 957.7 \pm 0.3$ MeV and $\sigma = 7.9 \pm 0.3$ MeV, corresponding to the expected mass resolution in this region. For masses of 1280 MeV and 1400 MeV, the expected resolutions are $\sigma = 20$ MeV and 24 MeV respectively.

4.2 Two–photon width

The $\eta\pi^+\pi^-$ mass spectrum for $P_T^2 < 0.02 \ \text{GeV}^2$ is shown in Figure 6b. No peak is seen in the region $1200-1480$ MeV. The detection efficiency is 2% and includes the trigger efficiency, which varies from 60% to 75%. Corrections for the inefficiencies due to higher level triggers range from 10% to 35%.

The absence of signals of $\eta(1440)$ and $\eta(1295)$ allows to calculate upper limits, at 95% CL on the $\eta\pi\pi$ decay. Taking into account the branching ratio $BR(\eta \to \gamma\gamma)$ [1] and the isospin factor $\eta\pi\pi \,/\, \eta\pi^+\pi^-$, they are:

$$\Gamma_{\gamma\gamma}\big(\eta(1440)\big) \times BR\big(\eta(1440) \to \eta\pi\pi\big) \;<\; 95 \ \text{eV} \,,$$

$$\Gamma_{\gamma\gamma}\big(\eta(1295)\big) \times \mathrm{BR}\big(\eta(1295) \to \eta\pi\pi\big) \quad < \quad 66 \text{ eV}.$$

They improve the limits of the Crystal Ball Collaboration [2].

The peak around 1285 MeV, seen in Figure 6a and absent in Figure 6b at $Q^2 \simeq 0$, is identified with the spin–1 state $f_1(1285)$. A Gaussian fit plus polynomial background gives $M = 1280 \pm 4$ MeV and $\sigma = 21 \pm 4$ MeV.

5 Discussion

The two–photon width of the $\eta(1440)$, calculated under the assumption that it is a member of the first radial excitation of the pseudoscalar nonet [19], is of the order of 0.1 keV. The $s\bar{s}$ content gives a negligible contribution. This is in agreement with our measurement, if we assume that $\mathrm{BR}\big(\eta(1440) \to \mathrm{K\bar{K}\pi}\big) \sim 100\%$.

If the $\eta(1440)$ we observe is a gluon rich state, its stickiness parameter [20] is expected to be large. The stickiness of a resonance R with mass m_R and two–photon width $\Gamma_{\mathrm{R}\to\gamma\gamma}$ is defined as:

$$\frac{|\langle \mathrm{R}|gg\rangle|^2}{|\langle \mathrm{R}|\gamma\gamma\rangle|^2} \sim S_\mathrm{R} = N_l \left(\frac{m_\mathrm{R}}{K_{\mathrm{J}\to\gamma\mathrm{R}}}\right)^{2l+1} \frac{\Gamma_{\mathrm{J}\to\gamma\mathrm{R}}}{\Gamma_{\mathrm{R}\to\gamma\gamma}},$$

where $K_{\mathrm{J}\to\gamma\mathrm{R}}$ is the energy of the photon in the J rest frame, l is the orbital angular momentum of the two initial photons or gluons ($l = 1$ for 0^-), $\Gamma_{\mathrm{J}\to\gamma\mathrm{R}}$ is the J radiative decay width for R, and N_l is a normalisation factor chosen to give $S_\eta = 1$. Using the present measurement of $\Gamma_{\gamma\gamma}\big(\eta(1440)\big) \times \mathrm{BR}\big(\eta(1440) \to \mathrm{K\bar{K}\pi}\big)$ and $\Gamma(\mathrm{J} \to \gamma\eta(1440)) = 79 \pm 16$ eV [1], a value of the stickiness $S_{\eta(1440)} = 79 \pm 26$ is obtained.

Another parameter, the gluiness (G), was introduced [21, 22] to quantify the ratio of the two–gluon and two–photon coupling of a particle, it is defined as:

$$G = \frac{9\, e_q^4}{2} \left(\frac{\alpha}{\alpha_s}\right)^2 \frac{\Gamma_{\mathrm{R}\to gg}}{\Gamma_{\mathrm{R}\to\gamma\gamma}},$$

where e_q is the relevant quark charge, calculated assuming equal amplitudes for $u\bar{u}$ and $d\bar{d}$ and zero amplitude for $s\bar{s}$. $\Gamma_{\mathrm{R}\to gg}$ is the two–gluon width of the resonance R, calculated from equation (3.4) of Reference [21]. Whereas stickiness is a relative measure, the gluiness is a normalised quantity and is expected to be near unity for a $q\bar{q}$ meson. Using the present measurement of $\Gamma_{\gamma\gamma}\big(\eta(1440)\big) \times \mathrm{BR}\big(\eta(1440) \to \mathrm{K\bar{K}\pi}\big)$ and the average value of $\alpha_s(1440 \text{ MeV}) = 0.369 \pm 0.022$ [1], a value $G_{\eta(1440)} = 41 \pm 14$ is obtained.

From the upper limit in the $\eta\pi^+\pi^-$ channel and the value $\Gamma(\mathrm{J} \to \gamma\eta(1440)) = 29 \pm 6$ eV [1] the limits $S_{\eta(1440)} > 87$ and $G_{\eta(1440)} > 45$ at 95% confidence level are obtained, compatible with the values obtained for the $\mathrm{K_S^0 K^\pm \pi^\mp}$ decay channel[3]. Both the stickiness and gluiness of the $\eta(1440)$ point to a large gluonium content in this resonance. For comparison, the η' pseudoscalar meson has $S_{\eta'} = 3.6 \pm 0.3$ and $G_{\eta'} = 5.2 \pm 0.8$ for $\alpha_s(958 \text{ MeV}) = 0.56 \pm 0.07$ [1].

6 Conclusions

The pseudoscalar meson $\eta(1440)$ is observed for the first time in $\gamma\gamma$ collisions. The two–photon width times branching ratio is measured to be $\Gamma_{\gamma\gamma}\big(\eta(1440)\big) \times \mathrm{BR}\big(\eta(1440) \to \mathrm{K\bar{K}\pi}\big) =$

---

[3] Although the coincidence can be fortuitous if these two final states correspond to two different pseudoscalars η_L and η_H.

212 ± 50 (stat.) ± 23 (sys.) eV. Its mass and width as well as the observation of a dominant K*(892)K decay are compatible with the characteristics of the η_H. The measured two-photon width is consistent with the value expected for a first radial excitation of the pseudoscalar nonet. At the same time tests designed to establish the gluon content of a resonance point to a strong gluonium admixture.

No positive signal is observed for the η_L state, either in the $K_S^0 K^\pm \pi^\mp$ channel, where there is no clear evidence for an $a_0(980)\pi$ decay, or in the $\eta\pi^+\pi^-$ channel. Upper limits for the two–photon width of the $\eta(1440)$ and the $\eta(1295)$ in the decay channel $\eta\pi^+\pi^-$ are determined.

The high Q^2 events show clear evidence for the formation of the axial vector mesons $f_1(1420)$ in the decay channel $K_S^0 K^\pm \pi^\mp$ and for the formation of $f_1(1285)$ in both $K_S^0 K^\pm \pi^\mp$ and $\eta\pi^+\pi^-$ channels.

Acknowledgements

References

[1] D. .E. Groom *et al.* (Particle Data Group), Eur. Phys. J. **C 15** (2000) 1.

[2] Crystal Ball Collaboration, D. Antreasyan *et al.*, Phys. Rev. **D 36** (1987) 2633.

[3] CELLO Collaboration, H. J. Behrend *et al.*, Z. Phys. **C 42** (1989) 367.

[4] OBELIX Collaboration, C. Cicalo *et al.*, Phys. Lett. **B 462** (1999) 453;
M. G. Rath *et al.*, Phys. Rev. **D 40** (1989) 693;
DM2 Collaboration, J. E. Augustin *et al.*, Phys. Rev. **D 46** (1992) 1951;
Mark III Collaboration, Z Bai *et al.*, Phys. Rev. Lett. **65** (1990) 2507.

[5] C. J. Morningstar and M. Pearon, Phys. Rev. **D 60** (1999) 034509;
UKQCD Collaboration, G. Bali *et al.* Phys. Lett. **B 309** (1993) 378.

[6] I. Campos *et al.*, Eur. Phys. J. **C 11** (1999) 507;
G. D. Farrar, Phys. Rev. Lett. **76** (1996) 4111.

[7] TPC-2γ Collaboration, H. Aihara *et al.*, Phys. Lett. **B 209** (1988) 107; Phys. Rev. **D 38** (1988) 1.

[8] JADE Collaboration, P. Hill *et al.*, Z. Phys. **C 42** (1989) 355.

[9] Mark II Collaboration, G. Gidal *et al.*, Phys. Rev. Lett. **59** (1987) 2012; Phys. Rev. Lett. **59** (1987) 2016.

[10] L3 Collaboration., B. Adeva *et al.*, Nucl. Inst. Meth. **A 289** (1990) 35; M. Acciarri *et al.*, Nucl. Inst. Meth. **A 351** (1994) 300; M. Chemarin *et al.*, Nucl. Inst. Meth. **A 349** (1994) 345; A. Adam *et al.*, Nucl. Inst. Meth. **A 383** (1996) 342; I. C. Brock *et al.*, Nucl. Inst. Meth. **A 381** (1996) 236.

[11] P. Béné *et al.*, Nucl. Inst. Meth. **A 306** (1991) 150; D. Haas *et al.*, Nucl. Inst. Meth. **A 420** (1999) 101.

[12] L. D. Landau, Dokl. Akad. Nauk. USSR **60** (1948) 207;
C. N. Yang, Phys. Rev. **77** (1950) 242.

[13] G. A. Schuler *et al.*, Nucl. Phys. **B 523** (1998) 423.

[14] F. L. Linde, *"Charm Production in Two–Photon Collisions"*, Ph. D. Thesis, Rijksuniversiteit Leiden, (1988).

[15] R. van Gulik, Nucl. Phys. **B 82** (Proc. Suppl.) (2000) 311.

[16] V. M. Budnev *et al.*, Phys. Rep. **C 15** (1975) 181.

[17] R. Brun *et al.*, GEANT 3.15 preprint CERN DD/EE/84-1 (Revised 1987).

[18] H. Fesefeldt, RWTH Aachen report PITHA 85/2 (1985).

[19] A. V. Anisovich *et al.*, Eur. Phys. J. **A 6** (1999) 247.

[20] M. Chanowitz, *in Proceedings of the VI International Workshop on Photon-Photon Collisions*, Lake Tahoe, California, 1984, edited by R. L. Lander (World Scientific, Singapore, 1985).

[21] F. E. Close, G. R. Farrar, Z. Li, Phys. Rev. **D 55** (1997) 5749.

[22] H. P. Paar, Nucl. Phys. **B 82** (Proc. Suppl.) (2000) 337.

The L3 Collaboration:

M.Acciarri,[26] P.Achard,[19] O.Adriani,[16] M.Aguilar-Benitez,[25] J.Alcaraz,[25] G.Alemanni,[22] J.Allaby,[17] A.Aloisio,[28] M.G.Alviggi,[28] G.Ambrosi,[19] H.Anderhub,[48] V.P.Andreev,[6,36] T.Angelescu,[12] F.Anselmo,[9] A.Arefiev,[27] T.Azemoon,[3] T.Aziz,[10] P.Bagnaia,[35] A.Bajo,[25] L.Baksay,[43] A.Balandras,[4] S.V.Baldew,[2] S.Banerjee,[10] Sw.Banerjee,[10] A.Barczyk,[48,46] R.Barillère,[17] P.Bartalini,[22] M.Basile,[9] N.Batalova,[45] R.Battiston,[32] A.Bay,[22] F.Becattini,[16] U.Becker,[14] F.Behner,[48] L.Bellucci,[16] R.Berbeco,[3] J.Berdugo,[25] P.Berges,[14] B.Bertucci,[32] B.L.Betev,[48] S.Bhattacharya,[10] M.Biasini,[32] A.Biland,[48] J.J.Blaising,[4] S.C.Blyth,[33] G.J.Bobbink,[2] A.Böhm,[1] L.Boldizsar,[13] B.Borgia,[35] D.Bourilkov,[48] M.Bourquin,[19] S.Braccini,[19] J.G.Branson,[39] F.Brochu,[4] A.Buffini,[16] A.Buijs,[44] J.D.Burger,[14] W.J.Burger,[32] X.D.Cai,[14] M.Capell,[14] G.Cara Romeo,[9] G.Carlino,[28] A.M.Cartacci,[16] J.Casaus,[25] G.Castellini,[16] F.Cavallari,[35] N.Cavallo,[37] C.Cecchi,[32] M.Cerrada,[25] F.Cesaroni,[23] M.Chamizo,[19] Y.H.Chang,[50] U.K.Chaturvedi,[18] M.Chemarin,[24] A.Chen,[50] G.Chen,[7] G.M.Chen,[7] H.F.Chen,[20] H.S.Chen,[7] G.Chiefari,[28] L.Cifarelli,[38] F.Cindolo,[9] C.Civinini,[16] I.Clare,[14] R.Clare,[14] G.Coignet,[4] N.Colino,[25] S.Costantini,[5] F.Cotorobai,[12] B.de la Cruz,[25] A.Csilling,[13] S.Cucciarelli,[32] T.S.Dai,[14] J.A.van Dalen,[30] R.D'Alessandro,[16] R.de Asmundis,[28] P.Déglon,[19] A.Degré,[4] K.Deiters,[46] D.della Volpe,[28] E.Delmeire,[19] P.Denes,[34] F.DeNotaristefani,[35] A.De Salvo,[48] M.Diemoz,[35] M.Dierckxsens,[2] D.van Dierendonck,[2] C.Dionisi,[35] M.Dittmar,[48] A.Dominguez,[39] A.Doria,[28] M.T.Dova,[18,♯] D.Duchesneau,[4] D.Dufournaud,[4] P.Duinker,[2] I.Duran,[40] H.El Mamouni,[24] A.Engler,[33] F.J.Eppling,[14] F.C.Erné,[2] P.Extermann,[19] M.Fabre,[46] M.A.Falagan,[25] S.Falciano,[35,17] A.Favara,[17] J.Fay,[24] O.Fedin,[36] M.Felcini,[48] T.Ferguson,[33] H.Fesefeldt,[1] E.Fiandrini,[32] J.H.Field,[19] F.Filthaut,[17] P.H.Fisher,[14] I.Fisk,[39] G.Forconi,[14] K.Freudenreich,[48] C.Furetta,[26] Yu.Galaktionov,[27,14] S.N.Ganguli,[10] P.Garcia-Abia,[5] M.Gataullin,[31] S.S.Gau,[11] S.Gentile,[35,17] N.Gheordanescu,[12] S.Giagu,[35] Z.F.Gong,[20] G.Grenier,[24] O.Grimm,[48] M.W.Gruenewald,[8] M.Guida,[38] R.van Gulik,[2] V.K.Gupta,[34] A.Gurtu,[10] L.J.Gutay,[45] D.Haas,[5] A.Hasan,[29] D.Hatzifotiadou,[9] T.Hebbeker,[8] A.Hervé,[17] P.Hidas,[13] J.Hirschfelder,[33] H.Hofer,[48] G. Holzner,[48] H.Hoorani,[33] S.R.Hou,[50] Y.Hu,[30] I.Iashvili,[47] B.N.Jin,[7] L.W.Jones,[3] P.de Jong,[2] I.Josa-Mutuberría,[25] R.A.Khan,[18] M.Kaur,[18,♢] M.N.Kienzle-Focacci,[19] D.Kim,[35] J.K.Kim,[42] J.Kirkby,[17] D.Kiss,[13] W.Kittel,[30] A.Klimentov,[14,27] A.C.König,[30] M.Kopal,[45] A.Kopp,[47] V.Koutsenko,[14,27] M.Kräber,[48] R.W.Kraemer,[33] W.Krenz,[1] A.Krüger,[47] A.Kunin,[14,27] P.Ladron de Guevara,[25] I.Laktineh,[24] G.Landi,[16] M.Lebeau,[17] A.Lebedev,[14] P.Lebrun,[24] P.Lecomte,[48] P.Lecoq,[17] P.Le Coultre,[48] H.J.Lee,[8] J.M.Le Goff,[17] R.Leiste,[47] P.Levtchenko,[36] C.Li,[20] S.Likhoded,[47] C.H.Lin,[50] W.T.Lin,[50] F.L.Linde,[2] L.Lista,[28] Z.A.Liu,[7] W.Lohmann,[47] E.Longo,[35] Y.S.Lu,[7] K.Lübelsmeyer,[1] C.Luci,[17,35] D.Luckey,[14] L.Lugnier,[24] L.Luminari,[35] W.Lustermann,[48] W.G.Ma,[20] M.Maity,[10] L.Malgeri,[17] A.Malinin,[17] C.Maña,[25] D.Mangeol,[30] J.Mans,[34] G.Marian,[15] J.P.Martin,[24] F.Marzano,[35] K.Mazumdar,[10] R.R.McNeil,[6] S.Mele,[17] L.Merola,[28] M.Meschini,[16] W.J.Metzger,[30] M.von der Mey,[1] A.Mihul,[12] H.Milcent,[17] G.Mirabelli,[35] J.Mnich,[1] G.B.Mohanty,[10] T.Moulik,[10] G.S.Muanza,[24] A.J.M.Muijs,[2] B.Musicar,[39] M.Musy,[35] M.Napolitano,[28] F.Nessi-Tedaldi,[48] H.Newman,[31] T.Niessen,[1] A.Nisati,[35] H.Nowak,[47] R.Ofierzynski,[48] G.Organtini,[35] A.Oulianov,[27] C.Palomares,[25] D.Pandoulas,[1] S.Paoletti,[35,17] P.Paolucci,[28] R.Paramatti,[35] H.K.Park,[33] I.H.Park,[42] G.Passaleva,[17] S.Patricelli,[28] T.Paul,[11] M.Pauluzzi,[32] C.Paus,[17] F.Pauss,[48] M.Pedace,[35] S.Pensotti,[26] D.Perret-Gallix,[4] B.Petersen,[30] D.Piccolo,[28] F.Pierella,[9] M.Pieri,[16] P.A.Piroué,[34] E.Pistolesi,[26] V.Plyaskin,[27] M.Pohl,[19] V.Pojidaev,[27,16] H.Postema,[14] J.Pothier,[17] D.O.Prokofiev,[45] D.Prokofiev,[36] J.Quartieri,[38] G.Rahal-Callot,[48,17] M.A.Rahaman,[10] P.Raics,[15] N.Raja,[10] R.Ramelli,[48] P.G.Rancoita,[26] R.Ranieri,[16] A.Raspereza,[47] G.Raven,[39] P.Razis,[29] D.Ren,[48] M.Rescigno,[35] S.Reucroft,[11] S.Riemann,[47] K.Riles,[3] J.Rodin,[43] B.P.Roe,[3] L.Romero,[25] A.Rosca,[8] S.Rosier-Lees,[4] J.A.Rubio,[17] G.Ruggiero,[16] H.Rykaczewski,[48] S.Saremi,[6] S.Sarkar,[35] J.Salicio,[17] E.Sanchez,[17] M.P.Sanders,[30] C.Schäfer,[17] V.Schegelsky,[36] S.Schmidt-Kaerst,[1] D.Schmitz,[1] H.Schopper,[49] D.J.Schotanus,[30] G.Schwering,[1] C.Sciacca,[28] A.Seganti,[9] L.Servoli,[32] S.Shevchenko,[31] N.Shivarov,[41] V.Shoutko,[27] E.Shumilov,[27] A.Shvorob,[31] T.Siedenburg,[1] D.Son,[42] B.Smith,[33] P.Spillantini,[16] M.Steuer,[14] D.P.Stickland,[34] A.Stone,[6] B.Stoyanov,[41] A.Straessner,[1] K.Sudhakar,[10] G.Sultanov,[18] L.Z.Sun,[20] S.Sushkov,[8] H.Suter,[48] J.D.Swain,[18] Z.Szillasi,[43,¶] T.Sztaricskai,[43,¶] X.W.Tang,[7] L.Tauscher,[5] L.Taylor,[11] B.Tellili,[24] C.Timmermans,[30] Samuel C.C.Ting,[14] S.M.Ting,[14] S.C.Tonwar,[10] J.Tóth,[13] C.Tully,[17] K.L.Tung,[7] Y.Uchida,[14] J.Ulbricht,[48] E.Valente,[35] G.Vesztergombi,[13] I.Vetlitsky,[27] D.Vicinanza,[38] G.Viertel,[48] S.Villa,[11] M.Vivargent,[4] S.Vlachos,[5] I.Vodopianov,[36] H.Vogel,[33] H.Vogt,[47] I.Vorobiev,[33] A.A.Vorobyov,[36] A.Vorvolakos,[29] M.Wadhwa,[5] W.Wallraff,[1] M.Wang,[14] X.L.Wang,[20] Z.M.Wang,[20] A.Weber,[1] M.Weber,[1] P.Wienemann,[1] H.Wilkens,[30] S.X.Wu,[14] S.Wynhoff,[17] L.Xia,[31] Z.Z.Xu,[20] J.Yamamoto,[3] B.Z.Yang,[20] C.G.Yang,[7] H.J.Yang,[7] M.Yang,[7] J.B.Ye,[20] S.C.Yeh,[51] An.Zalite,[36] Yu.Zalite,[36] Z.P.Zhang,[20] G.Y.Zhu,[7] R.Y.Zhu,[31] A.Zichichi,[9,17,18] G.Zilizi,[43,¶] B.Zimmermann,[48] M.Zöller.[1]

1 I. Physikalisches Institut, RWTH, D-52056 Aachen, FRG[§]
   III. Physikalisches Institut, RWTH, D-52056 Aachen, FRG[§]
2 National Institute for High Energy Physics, NIKHEF, and University of Amsterdam, NL-1009 DB Amsterdam, The Netherlands
3 University of Michigan, Ann Arbor, MI 48109, USA
4 Laboratoire d'Annecy-le-Vieux de Physique des Particules, LAPP,IN2P3-CNRS, BP 110, F-74941 Annecy-le-Vieux CEDEX, France
5 Institute of Physics, University of Basel, CH-4056 Basel, Switzerland
6 Louisiana State University, Baton Rouge, LA 70803, USA
7 Institute of High Energy Physics, IHEP, 100039 Beijing, China[△]
8 Humboldt University, D-10099 Berlin, FRG[§]
9 University of Bologna and INFN-Sezione di Bologna, I-40126 Bologna, Italy
10 Tata Institute of Fundamental Research, Bombay 400 005, India
11 Northeastern University, Boston, MA 02115, USA
12 Institute of Atomic Physics and University of Bucharest, R-76900 Bucharest, Romania
13 Central Research Institute for Physics of the Hungarian Academy of Sciences, H-1525 Budapest 114, Hungary[‡]
14 Massachusetts Institute of Technology, Cambridge, MA 02139, USA
15 KLTE-ATOMKI, H-4010 Debrecen, Hungary[¶]
16 INFN Sezione di Firenze and University of Florence, I-50125 Florence, Italy
17 European Laboratory for Particle Physics, CERN, CH-1211 Geneva 23, Switzerland
18 World Laboratory, FBLJA Project, CH-1211 Geneva 23, Switzerland
19 University of Geneva, CH-1211 Geneva 4, Switzerland
20 Chinese University of Science and Technology, USTC, Hefei, Anhui 230 029, China[△]
22 University of Lausanne, CH-1015 Lausanne, Switzerland
23 INFN-Sezione di Lecce and Università Degli Studi di Lecce, I-73100 Lecce, Italy
24 Institut de Physique Nucléaire de Lyon, IN2P3-CNRS,Université Claude Bernard, F-69622 Villeurbanne, France
25 Centro de Investigaciones Energéticas, Medioambientales y Tecnologícas, CIEMAT, E-28040 Madrid, Spain[♭]
26 INFN-Sezione di Milano, I-20133 Milan, Italy
27 Institute of Theoretical and Experimental Physics, ITEP, Moscow, Russia
28 INFN-Sezione di Napoli and University of Naples, I-80125 Naples, Italy
29 Department of Natural Sciences, University of Cyprus, Nicosia, Cyprus
30 University of Nijmegen and NIKHEF, NL-6525 ED Nijmegen, The Netherlands
31 California Institute of Technology, Pasadena, CA 91125, USA
32 INFN-Sezione di Perugia and Università Degli Studi di Perugia, I-06100 Perugia, Italy
33 Carnegie Mellon University, Pittsburgh, PA 15213, USA
34 Princeton University, Princeton, NJ 08544, USA
35 INFN-Sezione di Roma and University of Rome, "La Sapienza", I-00185 Rome, Italy
36 Nuclear Physics Institute, St. Petersburg, Russia
37 INFN-Sezione di Napoli and University of Potenza, I-85100 Potenza, Italy
38 University and INFN, Salerno, I-84100 Salerno, Italy
39 University of California, San Diego, CA 92093, USA
40 Dept. de Fisica de Particulas Elementales, Univ. de Santiago, E-15706 Santiago de Compostela, Spain
41 Bulgarian Academy of Sciences, Central Lab. of Mechatronics and Instrumentation, BU-1113 Sofia, Bulgaria
42 Laboratory of High Energy Physics, Kyungpook National University, 702-701 Taegu, Republic of Korea
43 University of Alabama, Tuscaloosa, AL 35486, USA
44 Utrecht University and NIKHEF, NL-3584 CB Utrecht, The Netherlands
45 Purdue University, West Lafayette, IN 47907, USA
46 Paul Scherrer Institut, PSI, CH-5232 Villigen, Switzerland
47 DESY, D-15738 Zeuthen, FRG
48 Eidgenössische Technische Hochschule, ETH Zürich, CH-8093 Zürich, Switzerland
49 University of Hamburg, D-22761 Hamburg, FRG
50 National Central University, Chung-Li, Taiwan, China
51 Department of Physics, National Tsing Hua University, Taiwan, China

State	Mass (MeV)	Width (MeV)
$\eta_L \to \eta\pi\pi$	1405 ± 5	56 ± 7
$\eta_L \to K\bar{K}\pi$	1418 ± 1	58 ± 4
$\eta_H \to K\bar{K}\pi$	1475 ± 5	81 ± 11

Table 1: Average masses and widths for the pseudoscalars in the 1440 MeV region [1].

ΔP_T^2 (GeV^2)	Events	M (MeV)	σ (MeV)	CL (%)	ϵ (%)	$\Delta\sigma$ (pb)
$0 - 0.02$	37 ± 9	1481 ± 12	48 ± 9	89	1.03 ± 0.04	8.0 ± 2.0
$0.02 - 0.2$	28 ± 7	1473 ± 11	37 ± 8	77	0.85 ± 0.09	7.4 ± 2.3
$0.2 - 1.$	29 ± 9	1435 ± 10	32 ± 10	99	1.74 ± 0.14	3.7 ± 1.2
$1 - 7$	21 ± 6	1452 ± 11	35 ± 10	55	3.49 ± 0.24	1.4 ± 0.4
$1 - 7$	10 ± 4	1290 ± 12	29 ± 10		—	—

Table 2: Results of the Gaussian plus polynomial background fits performed on the mass spectra of Figure 3. The number of the events in the Gaussian, the mass M and the width σ are listed with the error given by the fit. All fits reproduce the data well, as proven by the confidence level (CL) value. The partial efficiency ϵ and the partial cross-section $\Delta\sigma$ (errors include systematic uncertainties) are also given for each P_T^2 interval.
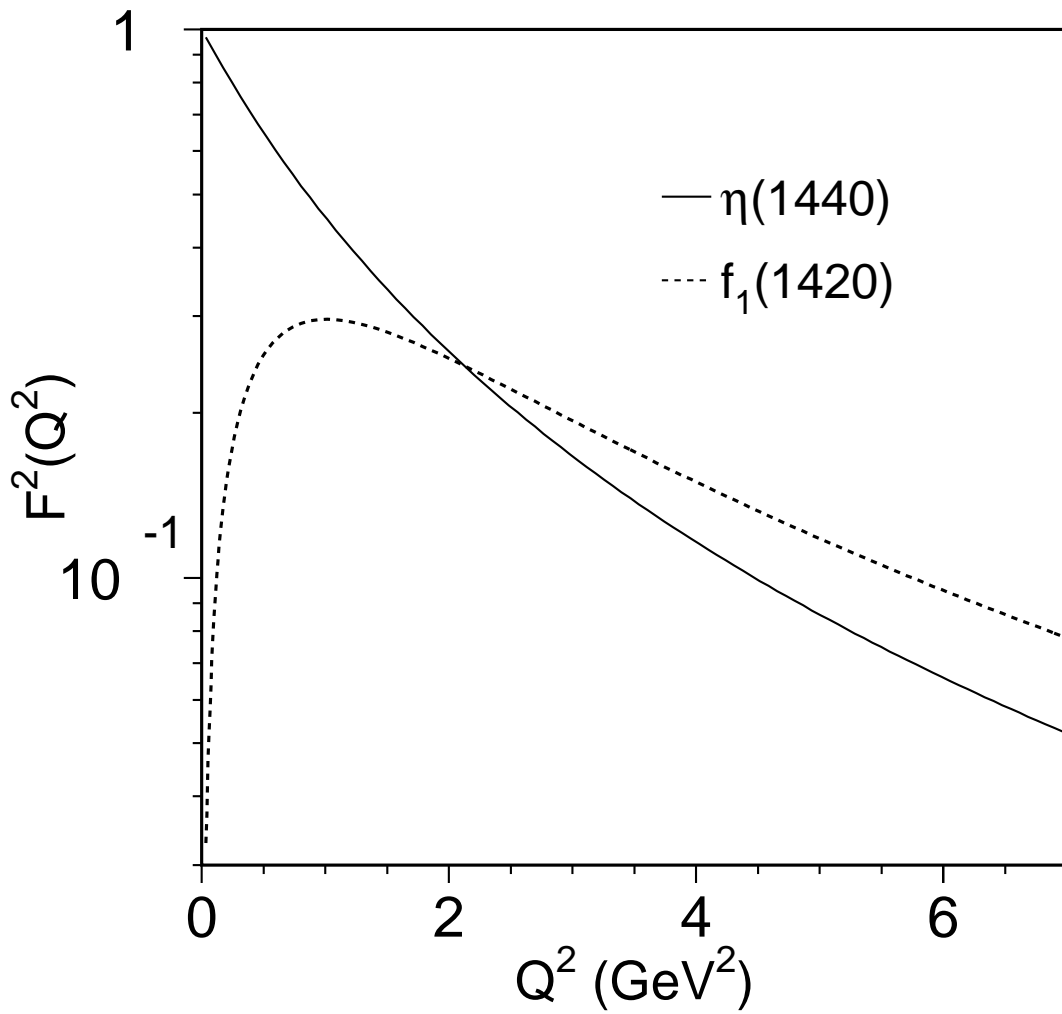
Figure 1: The form factors squared for $\eta(1440)$ (solid line) and $f_1(1420)$ (dashed line) in two–photon formation.
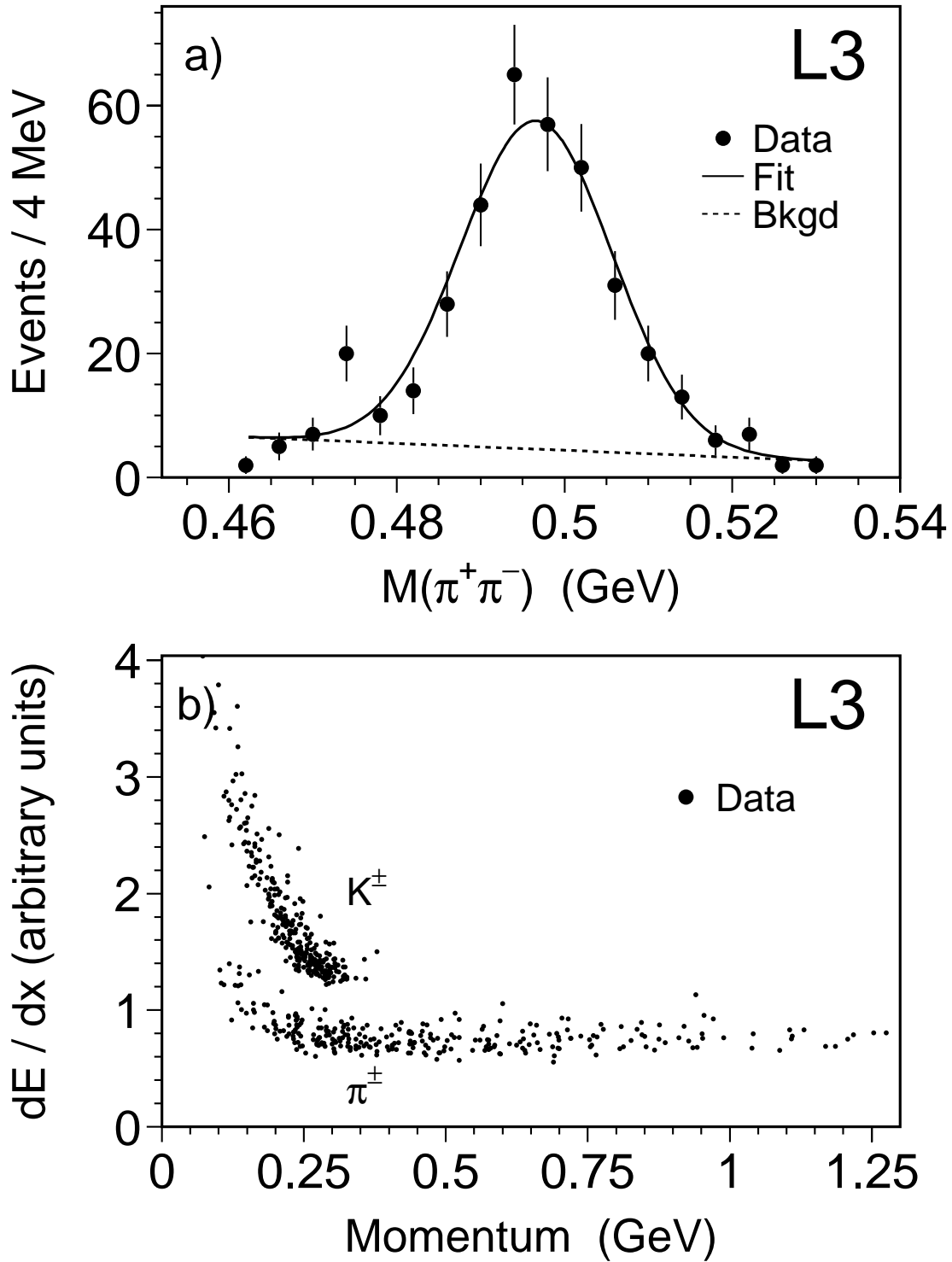
Figure 2: The $K_S^0 K^\pm \pi^\mp$ selection for $P_T^2 < 0.2$ GeV^2. a) The K_S^0 mass spectrum as the invariant mass of $\pi^+ \pi^-$ coming from the secondary vertex. b) dE/dx of charged kaons and pions at the primary vertex.
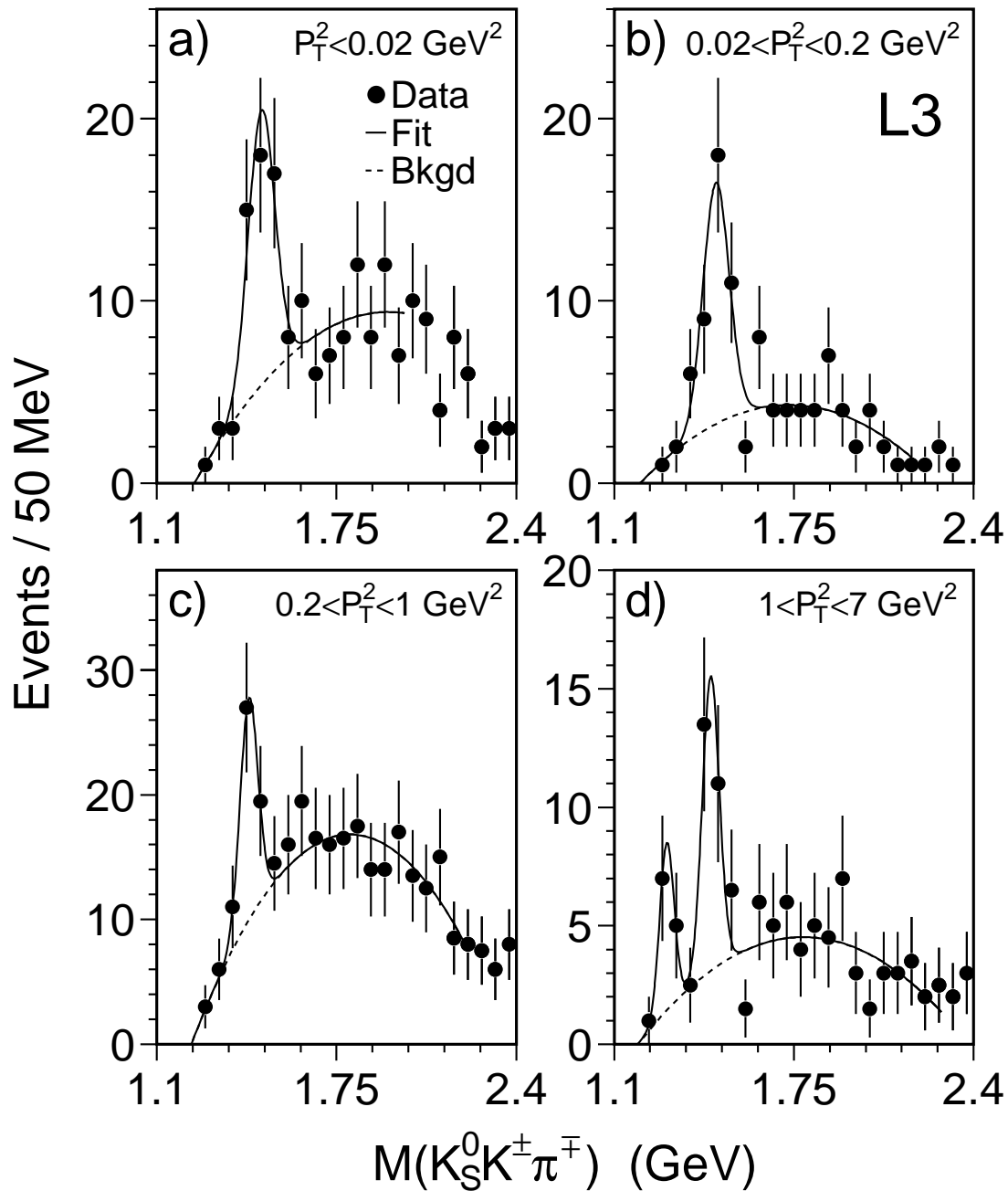
Figure 3: $K_S^0 K^\pm \pi^\mp$ spectra for different P_T^2 bins. The fits of a Gaussian plus polynomial background are superimposed on the data. In the highest P_T^2 bin, also the peak of the $f_1(1285)$ is present and the fit includes two Gaussians.
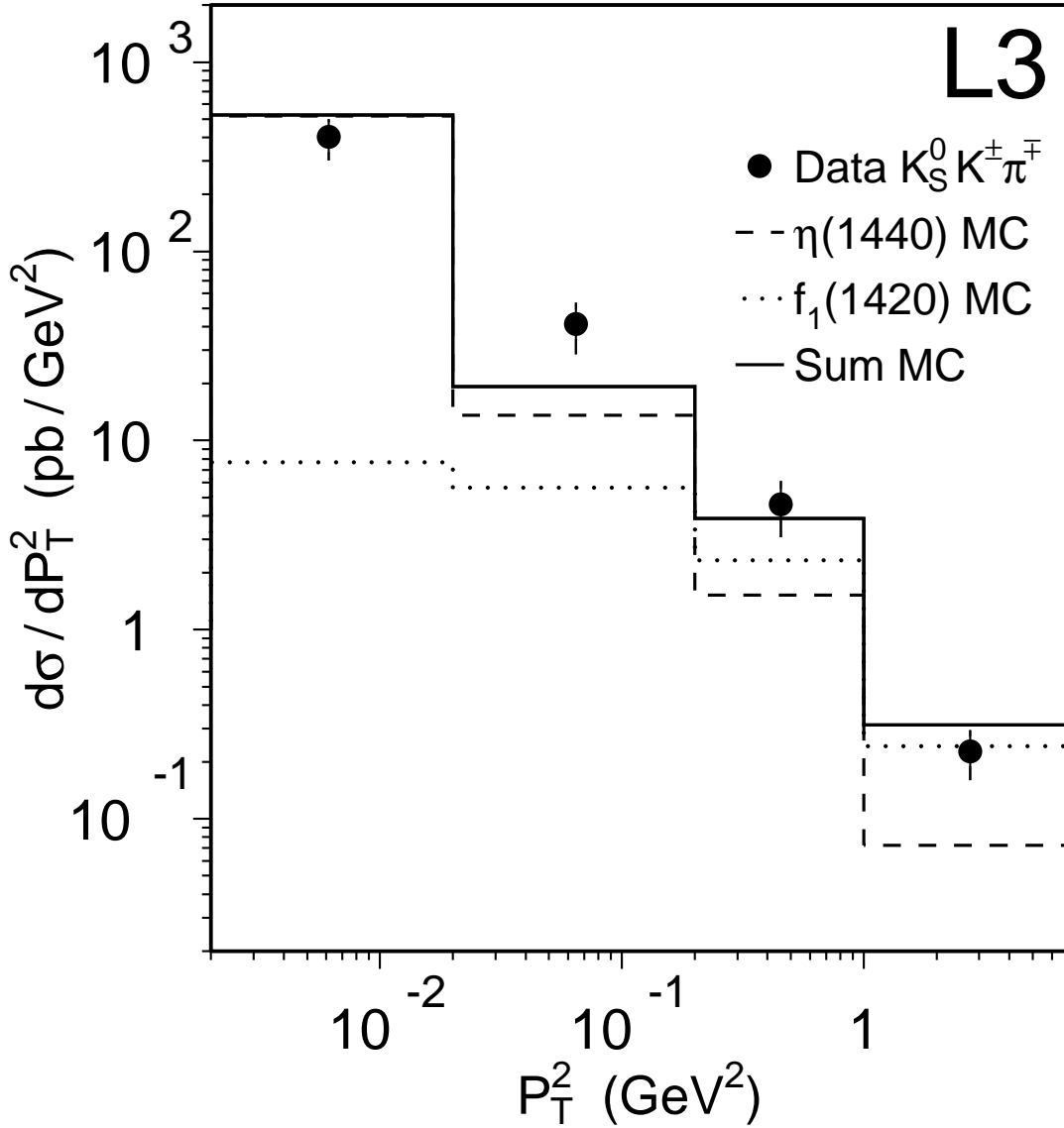
Figure 4: Differential cross section for the 1440 MeV mass region, as estimated from the Gaussian fit, as a function of P_T^2 in the $K_S^0 K^\pm \pi^\mp$ channel. The solid line is the sum of the $\eta(1440)$ and $f_1(1420)$ simulations fitted to the data. The partial contributions of $\eta(1440)$ (dashed line) and $f_1(1420)$ (dotted line) are also shown.
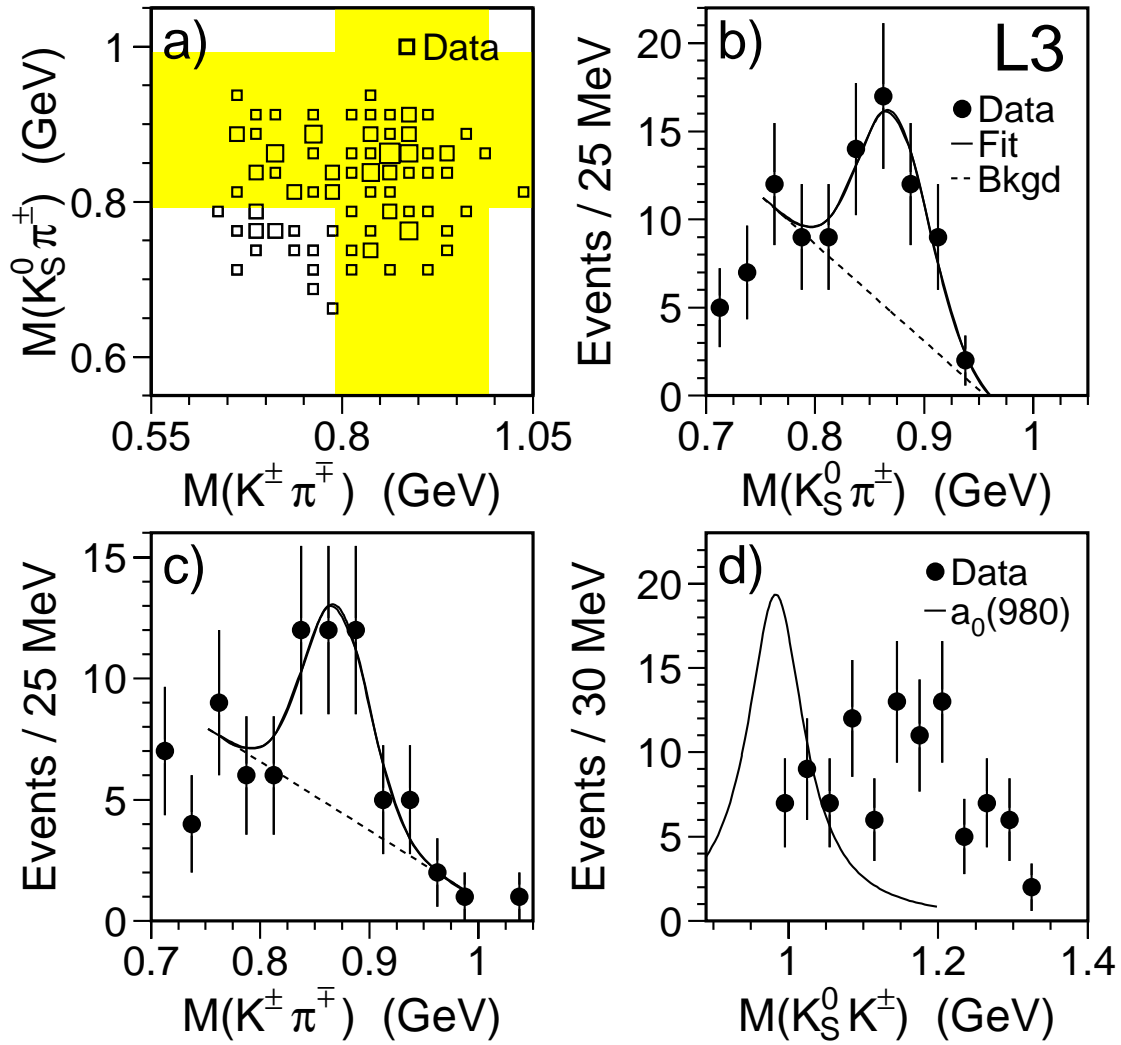
Figure 5: Search for the K*(892)K and $a_0(980)\pi$ states in the $K_S^0 K^\pm \pi^\mp$ sample for $P_T^2 <$ 0.2 GeV^2 in the $\eta(1440)$ region (1370–1560 MeV). The shadowed area displays the K*(892) bands (792 MeV $< M(K\pi) <$ 992 MeV). a) The scatter plot of Kπ combinations. b) and c) are the Kπ projections fitted with a Gaussian over a linear background. d) The $K_S^0 K^\pm$ mass spectrum; the Breit–Wigner function with the $a_0(980)$ parameters is drawn with arbitrary normalisation.
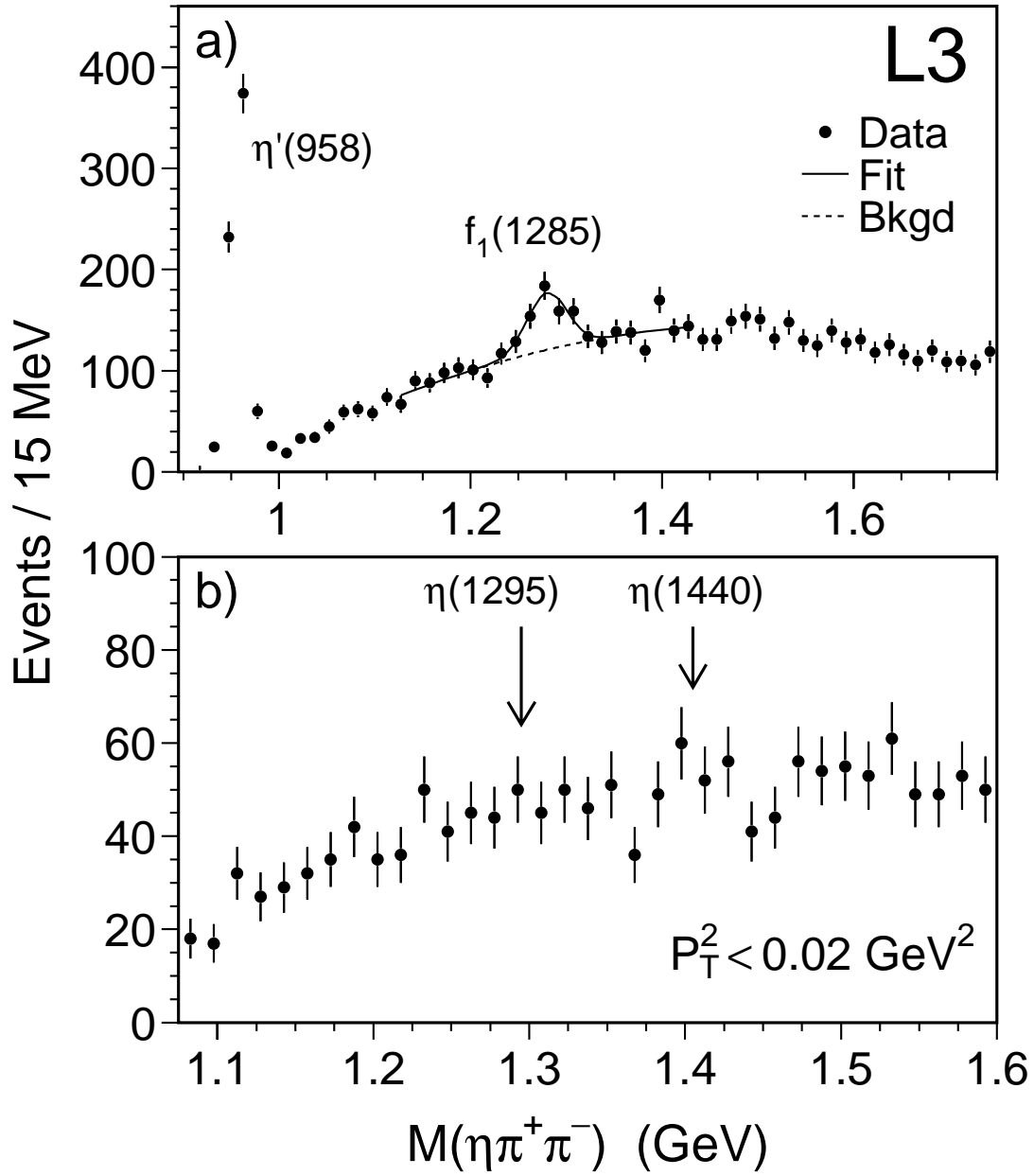
Figure 6: The $\eta\pi^+\pi^-$ mass spectra: a) total spectrum, the fit of a Gaussian plus polynomial background for the f$_1$(1285) region is superimposed on the data; b) for $P_T^2 < 0.02$ GeV^2, arrows show the location of $\eta(1295)$ and $\eta(1440)$.